Earth and Planetary Science Letters 426 (2015) 204–215

Contents lists available at ScienceDirect

Earth and Planetary Science Letters

www.elsevier.com/locate/epsl

Elasticity of single-crystal olivine at high pressures and temperatures

Zhu Mao [a,b,c,*], Dawei Fan [c,d,e], Jung-Fu Lin [c,e], Jing Yang [c], Sergey N. Tkachev [f], Kirill Zhuravlev [f], Vitali B. Prakapenka [f]

[a] Laboratory of Seismology and Physics of Earth's Interior, School of Earth and Space Sciences, University of Science and Technology of China, Hefei, Anhui 230026, China
[b] National Geophysical Observatory at Mengcheng, Anhui 233500, China
[c] Department of Geological Sciences, Jackson School of Geosciences, The University of Texas at Austin, Austin, TX 78712, USA
[d] Key Laboratory for High Temperature and High Pressure Study of the Earth's Interior of Institute of Geochemistry, CAS, Guiyang, Guizhou 550002, China
[e] Center for High Pressure Science and Technology Advanced Research (HPSTAR), Changchun, Jilin 130012, China
[f] Center for Advanced Radiation Sources, University of Chicago, Chicago, IL 60637, USA

ARTICLE INFO

Article history:
Received 25 December 2014
Received in revised form 21 June 2015
Accepted 23 June 2015
Available online xxxx
Editor: J. Brodholt

Keywords:
elasticity of single crystal
San Carlos olivine
high pressure and temperature
metastable olivine wedge
mantle
seismic anisotropy

ABSTRACT

Elasticity of single-crystal San Carlos olivine has been derived from sound velocity and density measurements at simultaneous high pressure–temperature conditions up to 20 GPa and 900 K using in situ Brillouin spectroscopy and single-crystal X-ray diffraction in externally-heated diamond anvil cells. These experimental results are used to evaluate the combined effect of pressure and temperature on full elastic constants of single-crystal olivine to better understand its velocity profiles and anisotropies in the deep mantle. Analysis of the results shows that the shear moduli display strong concave behaviors as a function of pressure at a given high temperature, while the longitudinal modulus, C_{11}, and the off-diagonal moduli, C_{12} and C_{13}, exhibit greater temperature dependence at higher pressures than at relatively lower pressures. Using a finite-strain theory and thermal equation of state modeling for a pyrolitic mantle composition along an expected mantle geotherm, our results show that the magnitude of the V_P and V_S jumps at the 410-km depth are 6% and 6.4%, respectively, which are greater than that found in seismic observations, suggesting a mantle olivine content of 40–50 vol%, which is less than what is expected for the pyrolite model. Our modeled velocity profiles for a metastable olivine wedge in the subduction slabs along a representative cold slab geotherm are 6% and 10% lower than those of wadsleyite and ringwoodite, respectively, at corresponding depths of the normal mantle. Our modeled results also show that metastable olivine in the cold slabs could have strong V_P and V_S anisotropies. The maximum V_P anisotropy is estimated to be 19–22% at transition zone depth, whereas the maximum V_S splitting is 13–23% and increases with depth. As a result, the presence of a metastable olivine wedge at the transition zone depth would exhibit a seismic signature of low velocity and strong seismic anisotropy which are consistent with recent seismic observations for various locations of the slabs and can be used as mineral physics constraints for future seismic detections of the metastable olivine wedges in the deep mantle.

1. Introduction

Seismological studies have provided some of the most direct information for understanding the physical properties of the Earth's deep interior (e.g. Dziewonski and Anderson, 1981; Kennett et al., 1995; Romanowicz, 1991; van der Hilst et al., 2007). Interpretation of seismic images and profiles requires detailed knowledge of the elasticity of major mantle minerals at relevant pressure–temperature (P–T) conditions (Bass et al., 2008; Cammarano et al., 2005a; Duffy and Anderson, 1989; Ita and Stixrude, 1992; Marquardt et al., 2009; Murakami et al., 2012). As one of the most abundant minerals in the Earth's upper mantle, olivine has the volume percentage of 60% in a pyrolitic mantle composition (Ringwood, 1975). Studying the elasticity of olivine at P–T conditions relevant to the Earth's mantle is of fundamental importance in constraining the composition and understanding the structure of the region.

* Corresponding author at: Laboratory of Seismology and Physics of Earth's Interior, School of Earth and Space Sciences, University of Science and Technology of China, Hefei, Anhui 230026, China.
E-mail address: zhumao@ustc.edu.cn (Z. Mao).

http://dx.doi.org/10.1016/j.epsl.2015.06.045
0012-821X/

Experimental studies on the elasticity of olivine date back to 1930s when Adams (1931) studied the compressibility of fayalite, an Fe-endmember olivine (Fe_2SiO_4), at ambient temperature. With the development of high pressure techniques, the elasticity of olivine was extensively studied at high pressures and 300 K or high temperatures and 1 bar in the past few decades (Abramson et al., 1997; Duffy et al., 1995; Webb, 1989; Zha et al., 1996, 1998). Although Liu et al. (2005) reported the aggregate bulk and shear moduli of San Carlos olivine at simultaneous high P–T conditions up to 8 GPa and 1073 K using ultrasonic interferometry technique, in situ high P–T measurements on the elasticity of single-crystal olivine remain unavailable. Much of our understanding of upper-mantle seismic structures and mineralogy still heavily relies on the extrapolated elasticity of the candidate upper-mantle minerals, including olivine, enstatite, and garnet (e.g. Abramson et al., 1997; Chai et al., 1997; Duffy and Anderson, 1989; Duffy et al., 1995; Jackson et al., 2007; Jiang et al., 2004a; Li and Liebermann, 2007; Webb, 1989; Zha et al., 1996, 1998). It is widely accepted that the olivine content in the upper mantle can be constrained by comparing the velocity contrast across the olivine–wadsleyite phase transition to seismic observations for the 410-km discontinuity (Cammarano et al., 2005b; Duffy et al., 1995; Liu et al., 2005). In this case, the olivine content in the upper mantle is estimated to be 30–50 vol%, a value much lower than 60 vol% in the pyrolite model. Such a low olivine content model challenges the traditional pyrolite compositional model and calls for an answer in order to reliably understand the upper mantle mineralogy (Cammarano et al., 2005b; Duffy et al., 1995; Li and Liebermann, 2007; Liu et al., 2005). The difference in the olivine content between these models could be attributed to our limited knowledge of the combined effect of P–T on the elasticity of olivine and wadsleyite at relevant mantle conditions. Therefore, high P–T measurements on the elasticity of olivine and other candidate mantle minerals are needed to provide a better constraint on the upper mantle mineralogy.

A considerable number of seismic studies have shown that Earth's upper mantle is seismically anisotropic in various locations (e.g. Assumpcao et al., 2006; Ekstrom and Dziewonski, 1998; Long and Becker, 2010; Long and van der Hilst, 2005; Marone and Romanowicz, 2007). In the upper 200–250 km depth, shear waves with horizontal polarization travel faster than waves with vertical polarization. This difference between two shear waves $[(V_{SH} - V_{SV})/V_{Voigt}\%]$ can reach up to 4% (Ekstrom and Dziewonski, 1998; Long and Becker, 2010; Marone and Romanowicz, 2007; Nettles and Dziewonski, 2008). Since olivine as a major mantle phase has been shown to be strongly anisotropic in both compressional (V_P) and shear wave (V_S) velocities, the observed anisotropy has been suggested to be caused by the preferred alignment of olivine fabrics (Jung et al., 2009; Karato et al., 2008; Mainprice et al., 2005). Knowledge of the elasticity of single-crystal olivine is thus the key to understanding the anisotropic seismic structures of the upper mantle (Mainprice, 2007; Mainprice et al., 2000; Nunez-Valdez et al., 2010; Zha et al., 1996). Furthermore, seismic anisotropies have also been observed in the subduction slabs in the transition zone and used as potential evidence for the presence of the metastable olivine wedge in the region (Chen and Brudzinski, 2003; Liu et al., 2008; Sandvol and Ni, 1997; Tono et al., 2009). We note that the phase transition of olivine to ringwoodite has been proposed to be a potential mechanism for occurrence of the deep earthquakes (e.g. Green et al., 2010; Green and Houston, 1995; Kirby, 1995). Knowing the elasticity of single-crystal olivine at P–T conditions relevant to the cold slab geotherm is thus essential for deciphering the seismic properties of the metastable olivine wedge. To date, there is no data available for the elasticity of single-crystal olivine at simultaneous high P–T (Abramson et al., 1997; Speziale et al., 2004; Webb, 1989; Zha et al., 1996, 1998), significantly hindering our progress in understanding the observed seismic anisotropy in the upper mantle and subduction slabs in the transition zone.

In this study, we have investigated the single-crystal elasticity of San Carlos olivine at simultaneous high P–T conditions using Brillouin spectroscopy combined with single-crystal X-ray diffraction (XRD) and externally-heated DACs (EHDAC) up to 20 GPa and 900 K. Using our experimental results, we have constructed a new velocity model in a pyrolite mantle composition to explore the nature of the 410-km discontinuity. We have also modeled the velocity and anisotropy profiles of the metastable olivine wedge in the subduction slabs to better understand its potential seismic structures in the transition zone.

2. Experimental details

Natural single-crystal San Carlos olivine $[(Mg_{0.9},Fe_{0.1})_2SiO_4]$ from Arizona, USA, was examined for the chemical composition using the electron microprobe at The University of Texas at Austin. The single crystal was cut into two pieces orthogonal to each other with random crystallographic orientations of $(0.96, 0.12, 0.24)$ (platelet 1) and $(0.49, -0.87, -0.03)$ (platelet 2), instead of with the principle orientations. For low-symmetry minerals, such as the orthorhombic olivine with nine independent elastic constants, a large number of velocity measurements from different crystallographic planes are typically needed to fully determine the elastic moduli of single crystals at a given P–T condition, though obtaining such measurements at extreme P–T is difficult in terms of the quantity of sample pieces and collection time needed. Compared to principle planes, crystal pieces in random orientations normally exhibit two polarized shear waves and one compressional wave velocity, which can be simultaneously used to greatly reduce the need for conducting extensive velocity measurements in various orientations. Such velocity measurements from two random orientations also provide excellent constraints on the values and uncertainties of the derived single-crystal elastic moduli (Mao et al., 2007; Speziale et al., 2004). Both of the randomly cut sample pieces were double-side polished to platelets of 30–35 μm in thickness and broken into several small platelets with a size of ~80 × 100 μm for the high P–T Brillouin and XRD measurements. Single-crystal XRD patterns were used to determine the orientations, crystal structure, and density of the sample at GeoSoilEnviroCARS (GSECARS) of the Advanced Photon Source (APS), Argonne National Laboratory (ANL). The starting sample had an orthorhombic structure with a density of 3.343(3) g/cm^3 at ambient conditions. Re–W alloy, which is more stable at high P–T conditions than typical Re gasket, was used as the gasket material for high P–T experiments. The gasket was pre-indented to a thickness of ~65 μm by a pair of diamonds of 500 μm culet size in an EHDAC, and a hole of 300 μm was subsequently drilled and used as the sample chamber. One selected platelet from each representative orientation of the olivine crystal was loaded into an EHDAC together with Pt powder which served as the pressure calibrant at high P–T (Fig. 1) (Fei et al., 2007). A ruby sphere of approximately 5 μm was also loaded into the cell and used as the pressure indicator for loading a Ne pressure medium as well as for high-pressure and room-temperature experiments. The temperature of the sample was determined by an R-type thermocouple attached to one of the diamond anvils approximately 500 μm away from the diamond culet. The EHDAC was equipped with an alumina ceramic heater that was coiled by two Pt wires of 200 μm in diameter and 30 cm in length (Kantor et al., 2012).

High P–T Brillouin measurements were conducted at up to 14 GPa at three given temperatures of 500 K, 750 K, and 900 K at GSECARS of the APS, ANL, while complimentary high-pressure

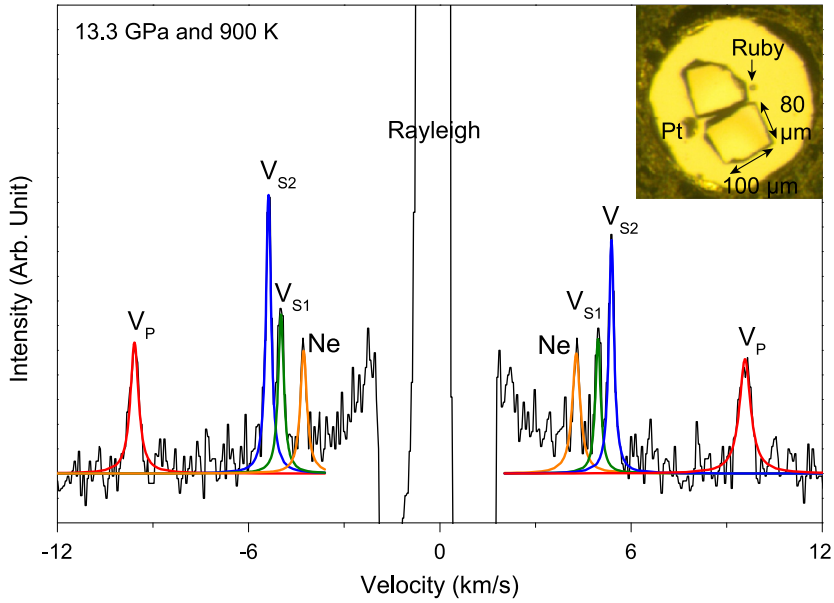

Fig. 1. Representative Brillouin spectrum of olivine at 13.3 GPa and 900 K. Black line: collected data; red, blue, green and orange lines: fitting results. Insert figure is a representative sample photo taken at ~6 GPa and 300 K. (For interpretation of the references to color in this figure legend, the reader is referred to the web version of this article.)

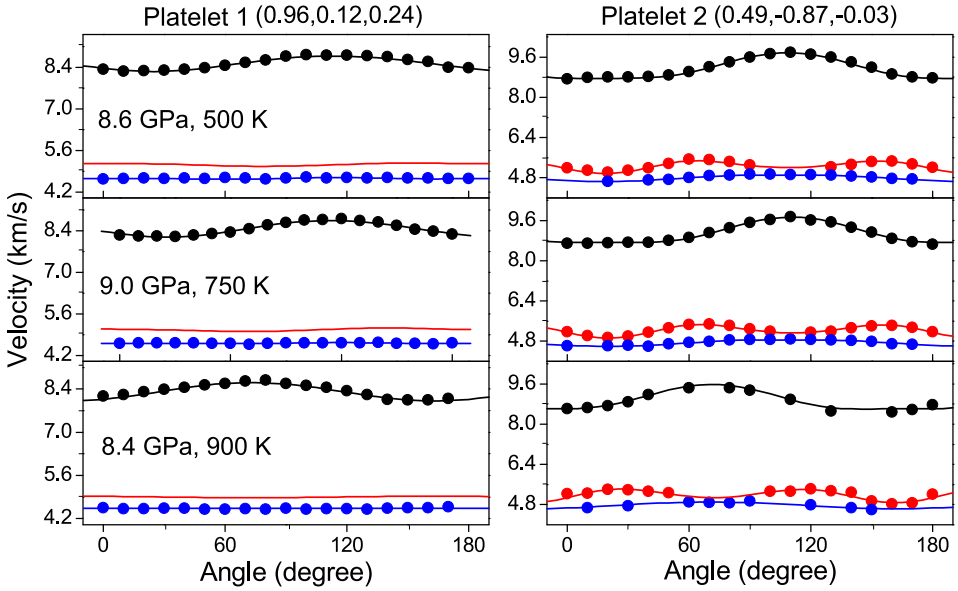

Fig. 2. Representative acoustic velocities of olivine measured at high P–T conditions as a function of azimuthal angles. Circles: measured velocities; lines: fitting results; black: quasi-longitudinal modes; red: fast quasi-shear mode; blue: slow quasi-shear mode. (For interpretation of the references to color in this figure legend, the reader is referred to the web version of this article.)

Brillouin measurements at room temperature were also performed up to 20 GPa at the Mineral Physics Laboratory of The University of Texas at Austin. To avoid potential oxidation of the diamond anvils and Pt wires at high temperatures, Ar with 2% hydrogen was continuously blown into the EHDAC while the cell was heated. A solid state laser with a wavelength of 532 nm and a power of 0.4 mW was used for the Brillouin measurements in which Brillouin spectra were collected at the forward scattering geometry with an external scattering angle of 50° using a six-pass Sandercock tandem Fabry–Perot interferometer. The acoustic velocities of the Brillouin spectra were derived from the measured Brillouin frequency shift as follows:

$$v = \frac{\Delta \upsilon_B \lambda_0}{2\sin(\theta/2)} \quad (1)$$

where v is the measured acoustic velocity, $\Delta\upsilon_B$ is the Brillouin frequency shift, λ_0 is the laser wavelength of 532 nm, and θ is the external scattering angle. For each platelet, we have collected the spectra at a 10° step vertically rotating over a range of 180° in the azimuthal direction (Fig. 1). For platelet 2, two quasi-transverse modes were observed for most directions, whereas only one quasi-transverse mode was detected in platelet 1 (Figs. 1 and 2). For the high-temperature measurements, the pressure was determined from the X-ray diffraction patterns of the Pt powder before and after each Brillouin measurement (Fei et al., 2007). We have also collected X-ray diffraction patterns of olivine at each given high P–T condition to determine the density of the sample. For the 300 K measurements at The University of Texas at Austin, the ruby fluorescence line was used to determine the pressure (Mao et al., 1986).

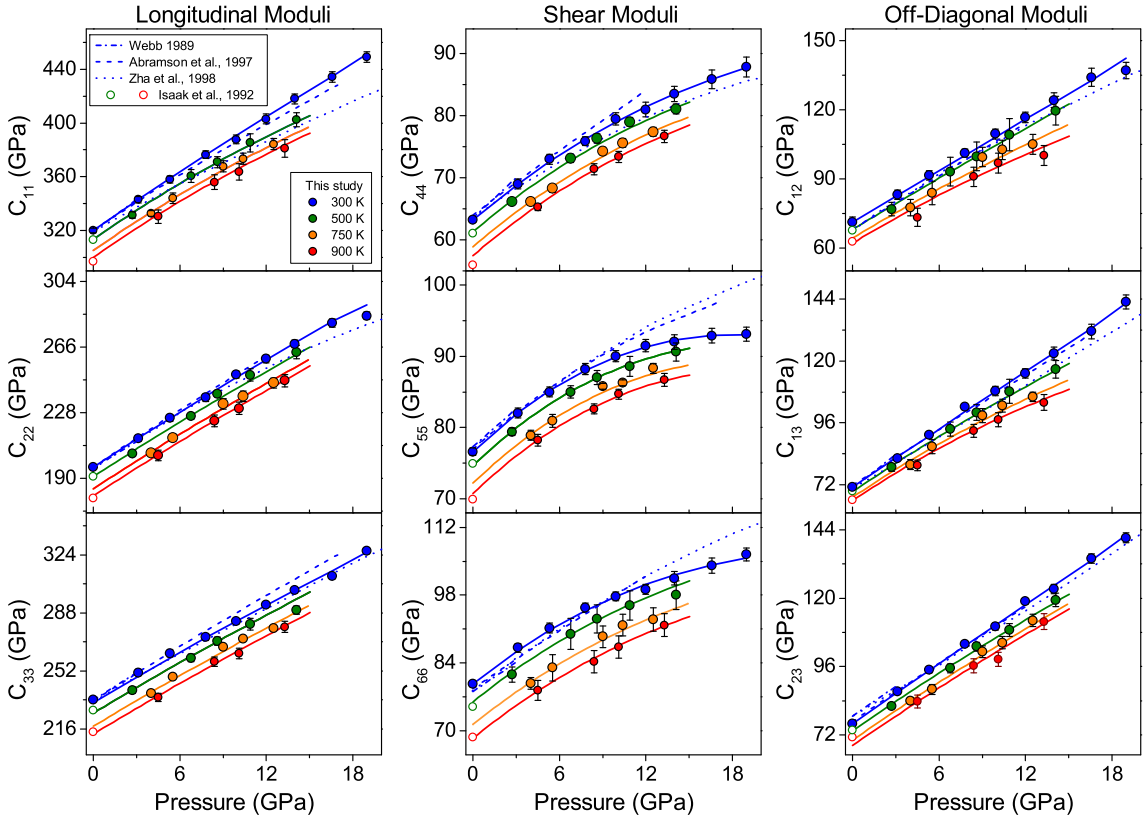

Fig. 3. Elastic moduli of single-crystal San Carlos olivine at high P–T. Blue: at 300 K; green: at 500 K; orange: at 750 K; red: at 900 K; solid circles: this study; open circles: Isaak (1992); dashed line: Abramson et al. (1997); dotted line: Zha et al. (1998); dashed–dotted line: Webb (1989). (For interpretation of the references to color in this figure legend, the reader is referred to the web version of this article.)

3. Results

At a given P–T condition, nine single-crystal elastic constants of olivine were obtained by simultaneously fitting the velocity data of two sample platelets with varying azimuthal angles using the Christoffel's equation (Figs. 2 and 3, Table S1) (Every, 1980):

$$|C_{ijkl}n_in_j - \rho v^2\delta_{ik}| = 0 \tag{2}$$

where v is the measured velocity, ρ is the density determined by single-crystal XRD, and δ_{ik} is the Kronecker delta function. The single-crystal elastic constants, C_{ijkl}, are written in full suffix notation in the equation, although we have used reduced notation, C_{ij}, for our reported values (Table S1). n_i represents the direction cosine of the phonon propagation direction, which can be described by three Eulerian angles (θ, χ, ϕ) and determined using single-crystal XRD measurements.

At 300 K, all of the longitudinal and off-diagonal moduli follow a nearly linear increase with pressure, whereas the shear moduli, C_{44}, C_{55}, and C_{66}, exhibit a downward trend towards higher pressures (Fig. 3). The aggregate bulk (K_S) and shear moduli (G) in the Voigt–Reuss–Hill average are then calculated using these single-crystal elastic moduli (Figs. 4 and 5). At ambient conditions, our Brillouin measurements yield the adiabatic bulk modulus, $K_{S0} = 129.8(9)$ GPa, and shear modulus, $G_0 = 77.8(5)$ GPa, which are in excellent agreement with literature results (Abramson et al., 1997). Although K_S increases almost linearly with pressure, G at 300 K exhibits a downward trend with pressure due to the softening of the shear moduli, C_{44}, C_{55}, and C_{66} (Figs. 4 and 5). Elevating temperature at a given pressure decreases all of the elastic moduli. In general, most of the elastic moduli exhibit similar pressure dependence at the investigated temperature range (Fig. 3 and Table S2). However, the off-diagonal moduli, C_{12} and C_{13}, show temperature-induced reduction more significantly at higher pressures (Fig. 3). The longitudinal modulus, C_{11}, also displays similar temperature-dependent trend at a higher pressure.

The P–T derivatives of the elastic moduli were obtained by fitting the experimentally-derived elastic constants using the third-order or fourth-order finite-strain equations as follows (Fig. 3 and Table S2) (Birch, 1978):

$$C_{ij0}(T) = C_{ij0}(300\text{ K}) + (T-300)(\partial C_{ij}/\partial T)_P \tag{3}$$

$$C_{ij} = (1+2f)^{7/2}\left[C_{ij0}(T) + a_1 f + a_2 f^2\right] + a_3 P \tag{4}$$

$$a_1 = 3K_{T0}\left(C''_{ij} - 3\right) - 7C_{ij0}(T) \tag{5}$$

$$a_2 = 9K_{T0}^2(T)C''_{ij} + K_{T0}(T)\left(9K'_{T0} - 48\right)\left(C'_{ij} - 3\right) + 63C_{ij0}(T) \tag{6}$$

$$f = (1/2)\left[(V_0/V)^{2/3} - 1\right] \tag{7}$$

where $C_{ij0}(300\text{ K})$ is the derived zero-pressure constant from ambient measurements and is thus fixed for the modeling, $C_{ij0}(T)$ is the elastic constant at high temperature and 1 bar, f is the finite strain, V is the volume at high P–T determined by single-crystal XRD, V_0 is the volume at 1 bar and high temperature, $C'_{ij} = (\partial C_{ij}/\partial P)_T$ is the pressure derivative of the elastic constants, $C''_{ij} = (\partial^2 C_{ij}/\partial^2 P)_T$ is the second pressure derivative of the elastic constants, $K_{T0}(T)$ is the isothermal bulk modulus at 1 bar and high temperature, $K'_{T0} = (\partial K_{T0}/\partial P)_T$ is the pressure derivative of the bulk modulus. The parameter a_3 is 3 for the longitudinal moduli, C_{11}, C_{22}, and C_{33}, and is 1 for the rest of the elastic moduli. $K_{T0}(T)$ and K'_{T0} are calculated from the adiabatic bulk modulus K_{S0} and K'_{S0} as follows:

$$K_{T0}(300\text{ K}) = K_{S0}/(1+\alpha\gamma T) \tag{8}$$

$$K_{T0}(T) = K_{T0}(300\text{ K}) + (\partial K_T/\partial T)_P(T-300) \tag{9}$$

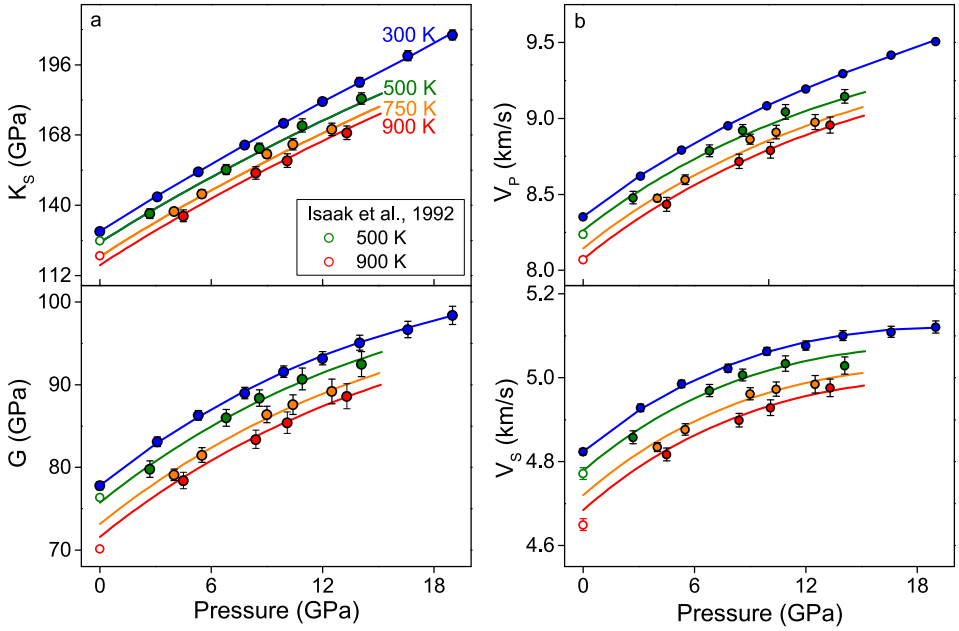

Fig. 4. Aggregate elastic moduli of San Carlos olivine at high pressures and temperatures. Blue: at 300 K; green: at 500 K; orange: at 750 K; red: at 900 K; solid circles: this study; open circles: Isaak (1992). (For interpretation of the references to color in this figure legend, the reader is referred to the web version of this article.)

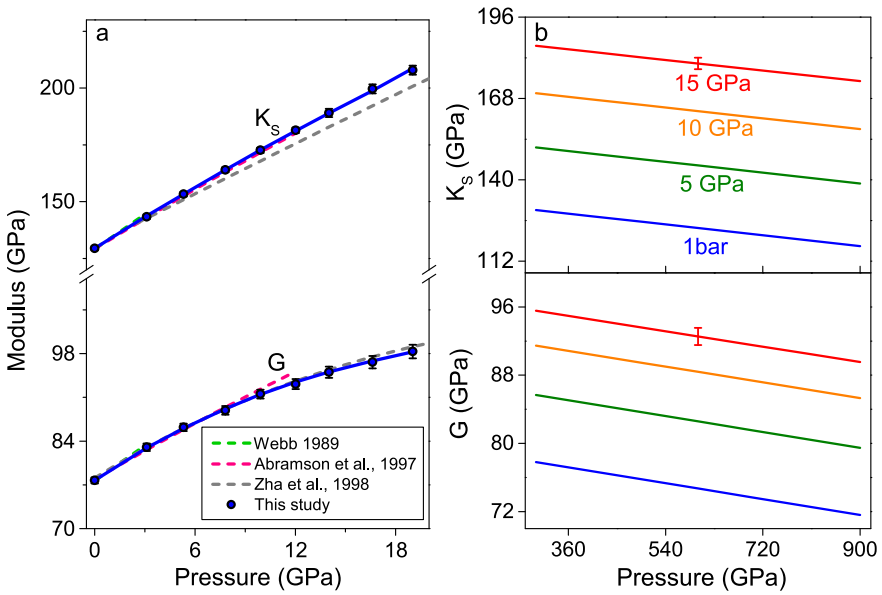

Fig. 5. Aggregate elastic moduli of San Carlos olivine. (a) At 300 K. Literature results are also plotted for comparison. Blue: this study; grey: Zha et al. (1998); orange: Abramson et al. (1997); green: Webb (1989). (b) Calculated with increasing temperature at a given pressure. (For interpretation of the references to color in this figure legend, the reader is referred to the web version of this article.)

$$K'_{T0} = (1+\alpha\gamma T)^{-1}\left[K'_{S0} - \gamma T/K_{T0}(T)(\partial K_T/\partial T)_P\right] \quad (10)$$

$$(\partial K_T/\partial T)_P \cong (\partial K_S/\partial T)_P/(1+\alpha\gamma T) - K_S(T)/(1+\alpha\gamma T)^2\left[\alpha\gamma + (\partial\alpha/\partial T)\gamma T\right] \quad (11)$$

Here we have used a literature value of 1.11 for the Gruneisen parameter, γ (Liu and Li, 2006). Fitting the K_S at high pressures and 300 K using the third finite equation with a fixed $K_{S0} = 129.8(9)$ GPa and a self-consistent density model (Speziale and Duffy, 2002), we have obtained $K'_{S0} = 4.45(5)$ (Figs. 4 and 5). The obtained K'_{S0} is slightly greater than that in the literature (Abramson et al., 1997; Zha et al., 1998). With the determined K'_{S0} value and high P–T K_S results, the temperature derivative of the bulk modulus, $(\partial K_S/\partial T)_P$, is determined to be $-0.020(2)$ GPa/K. The derived thermal expansion coefficient at ambient conditions is 3.47×10^{-5} K^{-1}.

As noted above, there is an enhanced effect of temperature on C_{12} and C_{13} towards higher pressures (Fig. 3). An extra term in the second pressure derivative of the C_{12} and C_{13} is needed in our modeling in order to fully describe the enhanced temperature dependence at higher pressures: $C''_{12} = -0.015 - 0.00021\times T$ (GPa/K), and $C''_{13} = -0.015 - 0.00021\times T$ (GPa/K). For C_{11}, the pressure derivative is derived from the high P–T data. The P–T derivatives of the shear modulus, G, are evaluated using the following equations:

$$G_0(T) = G_0(300\text{ K}) + (\partial G/\partial T)_P(T-300) \quad (12)$$

$$G = (1+2f)^{5/2}\left[G_0(T) + b_1 f + 1/2 b_2 f^2\right] \quad (13)$$

$$b_1 = 3K_{T0}(T)G_0' - 5G_0(T) \quad (14)$$

$$b_2 = 9\{K_{T0}^2(T)[G_0'' + 1/K_{T0}(T)(K_{T0}' - 4)G_0'] + 35G_0(T)/9\} \quad (15)$$

We thus obtain: $G_0' = 1.80(3)$, $G_0'' = -0.10(3)$ GPa^{-1} and $(\partial G/\partial T)_P = -0.010(2)$ GPa/K.

4. Discussion and geophysical implications

4.1. Single-crystal elasticity of olivine at high P–T

We have derived all of the nine elastic constants of single-crystal San Carlos olivine (Fig. 3 and Table S1). At ambient conditions, all of the elastic moduli are in excellent agreement with results in literature (Abramson et al., 1997; Webb, 1989; Zha et al., 1998). At 300 K, the longitudinal, off-diagonal and aggregate bulk moduli at high pressures are consistent with results by Abramson et al. (1997) and Webb (1989) within experimental uncertainties. Moreover, we have observed a softening in the shear moduli, C_{44}, C_{55}, C_{66} and G, with increasing pressure when approaching the olivine to wadsleyite phase transition (Fig. 3). Similar softening of elastic constants with pressure due to a structural phase transition has also been shown in other minerals, including stishovite, enstatite and orthoferrosilite (Kung and Li, 2014; Li et al., 2014; Yang and Wu, 2014). The softening of elastic constants, however, is not observed by Webb (1989) likely because of the limited experimental pressure range (up to 3 GPa). Abramson et al. (1997) reported the softening in C_{55}. However, other shear moduli, C_{44}, C_{66} and G, in Abramson et al. (1997) were only determined up to 12 GPa, where the softening started to occur. Although similar softening in the shear moduli has been shown by Zha et al. (1998) using the same Brillouin technique, C_{55} and C_{66} in this study exhibit a stronger downward curvature than those in Zha et al. (1998) (Fig. 3). Moreover, C_{11} and C_{13} at high pressures in Zha et al. (1998) are much lower than our results. To independently determine all elastic constants of minerals in the orthorhombic system, previous studies have shown that measuring velocities using platelets close to basal planes, such as (100), (010), and (001), permits reliable derivations of all elastic constants (Jiang et al., 2006; Speziale et al., 2004; Wang et al., 2014), because some of the longitudinal and/or shear moduli in such planes are not covariance with other elastic constants and can be better constrained. Even so, it is still necessary to measure the velocity in two or three different crystal planes, because single-crystal elastic moduli of a given orthorhombic mineral may not be well constrained when lacking sufficient velocity measurements (Every, 1980; Fan et al., accepted). It should be noted that the elastic moduli in Zha et al. (1998) were retrieved from the velocity data in the (111) plane with 19 measurements at each given pressure such that some of the obtained C_{ij}s in Zha et al. (1998) are expected to suffer from a stronger tradeoff with each other because these C_{ij}s cannot be well-constrained. Therefore, we have conducted our measurements using two platelets in different crystallographic orientations in which one platelet is close to the basal plane while another is a random plane in order to better constrain all nine elastic constants for the orthorhombic olivine crystal.

We have further compared our elasticity results to literature values for San Carlos olivine at high temperatures (Figs. 3 and 4, Table S2) (Isaak, 1992). Extrapolating our elastic constants at high P–T back to 1 bar and high temperature demonstrates agreement with Isaak (1992), with the exception of the effect of temperature on C_{44} and C_{23}. We note that the temperature derivatives at 1 bar and high temperatures for some of the elastic moduli (including C_{22}, C_{33}, C_{44}, C_{55}, and C_{66}) are indistinguishable from the values obtained from the high P–T measurements within experimental uncertainties (Table S2) (Isaak, 1992). However, the temperature dependence of C_{11} derived after considering the combined effect of P–T is smaller than the one at 1 bar and high temperatures, whereas the temperature dependence of C_{23} is larger. Of particular importance is the enhanced temperature dependence of the off-diagonal moduli, C_{12} and C_{13}, at high pressures. The softening behavior observed at high P–T may be associated with the olivine–wadsleyite transition that is prohibited because of the kinetic energy barrier (Kung and Li, 2014; Li et al., 2014; Yang and Wu, 2014). We have also plotted K_S and G as a function of temperature at various pressures to show the effect of temperature on the elasticity of olivine at a given pressure (Fig. 5). At the investigated P–T range, K_S and G exhibit a nearly linear decrease with increasing temperature at a given pressure.

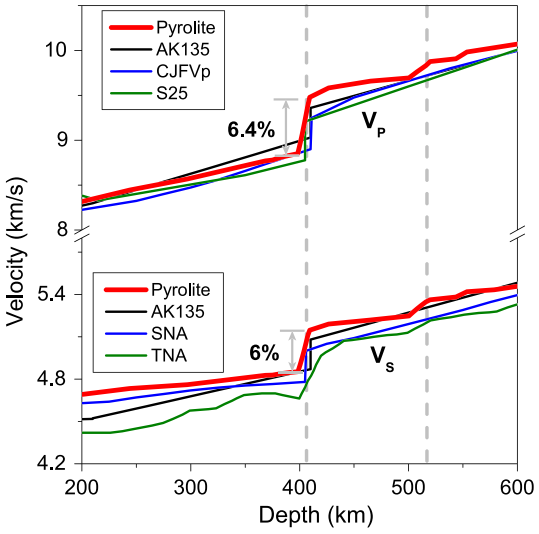

Fig. 6. Compressional (V_P) and shear wave (V_S) velocities of the mantle in a pyrolite composition compared with seismic profiles. Red line: calculated velocities of mantle in a pyrolite composition; black line: AK135 (Kennett et al., 1995); blue line of V_P: CJF (Walck, 1985); green line of V_P: S25 (Lefevre, 1989); blue line of V_S: SNA (Grand and Helmberger, 1984); green line of V_S: TNA (Grand and Helmberger, 1984). For modeling the elasticity of wadsleyite at relevant high pressure–temperature conditions of the transition zone, the effect of high pressure is taken from Wang et al. (2014), while the effect of temperature is from Isaak et al. (2010). (For interpretation of the references to color in this figure legend, the reader is referred to the web version of this article.)

4.2. The velocity contrast at the 410-km depth

The seismic 410-km discontinuity is associated with a 4–5% increase in V_P and a 4–4.6% increase in V_S, and it has been widely accepted to be caused by the olivine to wadsleyite phase transition (Grand and Helmberger, 1984; Kennett et al., 1995; Lefevre, 1989; Walck, 1985). A long-standing problem in mineral physics is that the calculated V_P and V_S jumps in a pyrolite composition using literature elasticity results of olivine and wadsleyite are 6–8% after accounting for their relative proportions. These values are greater than the aforementioned seismic discontinuities of 4–5% at the 410-km depth (Cammarano et al., 2005b; Duffy and Anderson, 1989; Li and Liebermann, 2007; Li et al., 2001). To understand the difference between the pyrolite model and seismic observations at the 410-km depth, we have constructed a new pyrolitic velocity model for the upper mantle and transition zone using our elasticity of olivine at high P–T (Fig. 6).

In the pyrolite compositional model, the volume percentage of olivine is approximately 60% (Ringwood, 1975), while pyroxene and garnet, so-called basaltic components, account for another 40% of the system (Irifune, 1987; Jeanloz and Thompson, 1983).

Table 1
Elasticity of minerals in the upper mantle and transition zone.

Mineral	ρ (g/cm^3)	K_{S0} (GPa)	K'_{S0}	$\partial K_S/\partial T$ (GPa/K)	$\partial^2 K_S/\partial T^2$ (GPa/K^2)	G (GPa)	G'_0	G'' (1/GPa)	$\partial G/\partial T$ (GPa/K)	$\partial^2 G/\partial T^2$ (GPa/K^2)
Olivine[a]	$3.227+0.012X_{Fe}$[i]	$128.8+0.08X_{Fe}$	4.47	−0.02		$81.6-0.38X_{Fe}$	1.8	−0.1	−0.01	
Wadsleyite[b]	$3.474+0.0159X_{Fe}$	170	4.2	−0.171		$112-0.4X_{Fe}$	1.4		−0.0157	
Ringwoodite[c]	$3.559+0.014X_{Fe}$	184	4.1	−0.021		$120-0.25X_{Fe}$	1.4		−0.016	
Clinopyroxene[d]	3.327	117.2	4.2	−0.013		72.2	1.4		−0.01	
Orthopyroxene[e]	3.306	115.5	7.82	−0.0238		78.1	1.45		−0.0125	
HP clinopyroxene[f]	3.45	156.7	5.5	−0.017		98.5	1.5		−0.015	
Pyrope garnet[g]	3.567	171.2	4.1	−0.0168		93.7	1.3		−0.0051	
Majorited-garnet[h]	3.605	164.4	4.2	−0.0091	-6×10^{-6}	94.9	1.1		−0.0074	-5×10^{-6}

[a] This study; Abramson et al. (1997); Zha et al. (1996).
[b] Isaak et al. (2007); Sinogeikin et al. (1998); Wang et al. (2014); Zha et al. (1997).
[c] Sinogeikin et al. (1998); Sinogeikin et al. (2003).
[d] Collins and Brown (1998); Duffy and Anderson (1989).
[e] Chai et al. (1997); Jackson et al. (2007); $K_S=115.4+7.82P-0.18P^2$.
[f] Kung et al. (2005).
[g] Sinogeikin and Bass (2000); Lu et al. (2013).
[h] Irifune et al. (2008).
[i] Fe content in mole%.

Olivine transforms into wadsleyite at approximately 410-km depth and to ringwoodite at around 520-km depth, whereas pyroxene and garnet transform into majorite in the upper mantle and transition zone (Fei and Bertka, 1999). In our modeling, we have taken into account the phase relations as a function of depth as well as the partitioning of Fe between olivine polymorphs and between olivine and residual basaltic components at the phase equilibria using previous experimental and theoretical results (Akaogi et al., 1989; Angel et al., 1992; Irifune, 1987; Irifune and Isshiki, 1998; Irifune and Ringwood, 1987; Katsura and Ito, 1989; Pacalo and Gasparik, 1990; Stixrude and Lithgow-Bertelloni, 2005; Xu et al., 2008). After considering the variation in phases and compositions with depth, the velocity of pyrolite has been constructed using the elasticity of olivine in this study and elasticity of other mantle phases in previous studies (Table 1) (Chai et al., 1997; Finger and Ohashi, 1976; Isaak et al., 2010; Jackson et al., 2003, 2007; Jiang et al., 2004b; Lu et al., 2013; Sang and Bass, 2014; Sinogeikin and Bass, 2000, 2002; Sinogeikin et al., 1998, 2001; Wang et al., 2014; Zhao et al., 1997; Zou et al., 2012).

The computed velocity model for a pyrolitic composition is compared to literature seismic profiles (Fig. 6). In general, the modeled V_P profile of the system is consistent with seismic observations in the upper mantle, whereas V_S is slightly larger. Karato (1993) has pointed out that the anelastic effects should be considered when applying the experimental data in interpreting the seismic velocities of the mantle. If we consider the anelastic effects due to temperature, the modeled V_S profile can decrease by 0.6–1.4%, leading to a V_S of the modeled pyrolitic mantle in a better agreement with seismic observations (Cammarano et al., 2003). However, due to the discrepancy in the attenuation profile of the upper mantle and transition zone in seismic studies (e.g. Romanowicz and Durek, 2000), the effect of anelasticity is not included in our modeling. On the other hand, a previous experimental study has shown that V_S of mantle minerals, such as majorite, could suffer from an enhanced non-linear reduction with increasing temperature at high pressures (Irifune et al., 2008). Taking this non-linear temperature effect at high pressures into account could lower the modeled V_P and V_S profiles to be in a better agreement with the seismic velocity profiles (Irifune et al., 2008). Although the elasticity of Fe-bearing olivine has been found to decrease linearly with temperature in both this study and previous experiments performed up to 1500 K and 1 bar (Isaak, 1992), it remains unclear whether or not the elasticity and sound velocities of olivine will suffer from a non-linear decrease with temperature above 900 K at high pressures. The aforementioned high-temperature effects on the attenuation and nonlinear velocity decrease should be further investigated in future studies in order to add to our understanding of the seismic features and mineralogical models of the region.

For the 410-km discontinuity, the olivine to wadsleyite phase transition produces a sharp velocity jump with a width of ~7 km (Fig. 6) (Frost, 2003). The calculated velocity jumps at the 410-km depth are 6.4% for V_P and 6% for V_S. Although the velocity jumps shown here are in a much better agreement with seismic observations as compared to previous velocity profiles for a pyrolitic upper mantle (Cammarano et al., 2005b; Duffy and Anderson, 1989; Li and Liebermann, 2007; Li et al., 2001), these values are still greater than the seismically-observed velocity increase of 4–5% at the 410-km depth (Grand and Helmberger, 1984; Kennett et al., 1995; Lefevre, 1989; Walck, 1985). To match a 4–5% velocity jump in seismic observations of the region, the olivine content in the mantle is estimated to be ~40–50 vol%, a value that is lower than what is expected for a pyrolitic compositional model; though, future elasticity studies at compatible P–T conditions of the mantle with higher accuracy are needed to better address this issue. On the other hand, the presence of water in the upper mantle and transition zone may help to reconcile some of the differences between the pyrolite model and seismic images (Jacobsen et al., 2008; Mao et al., 2008a, 2008b, 2011). Recent geological, mineralogical, and seismic studies have shown that various locations of the upper mantle and transition zone could be hydrated with up to 1 wt.% H_2O in ringwoodite (Pearson et al., 2014; Schmandt et al., 2014; Song et al., 2004; van der Meijde et al., 2003). Since hydration can cause a greater reduction in the velocity of wadsleyite than olivine at mantle P–T conditions, the presence of a certain amount of water in the mantle will lower the velocity jump at the 410-km depth (Jacobsen et al., 2008; Mao et al., 2008a, 2008b, 2010, 2011), therefore making the velocity of pyrolite agree better with seismic observations of the upper mantle and the transition zone (Mao et al., 2008a, 2008b, 2011). Future studies are needed to further examine the effect of water on the velocity of minerals in a pyrolitic composition in the upper mantle and transition zone.

4.3. Velocity profiles of the metastable olivine wedge in the subduction slabs

The metastable olivine wedge in the subducted mantle lithosphere has long been proposed to exist below the 410-km discontinuity due to the relatively cold nature of the slabs that kinetically inhibits the transformation of olivine to wadsleyite in the region. According to previous petrological studies, subducted mantle lithosphere consists of harzburgite at the top and less de-

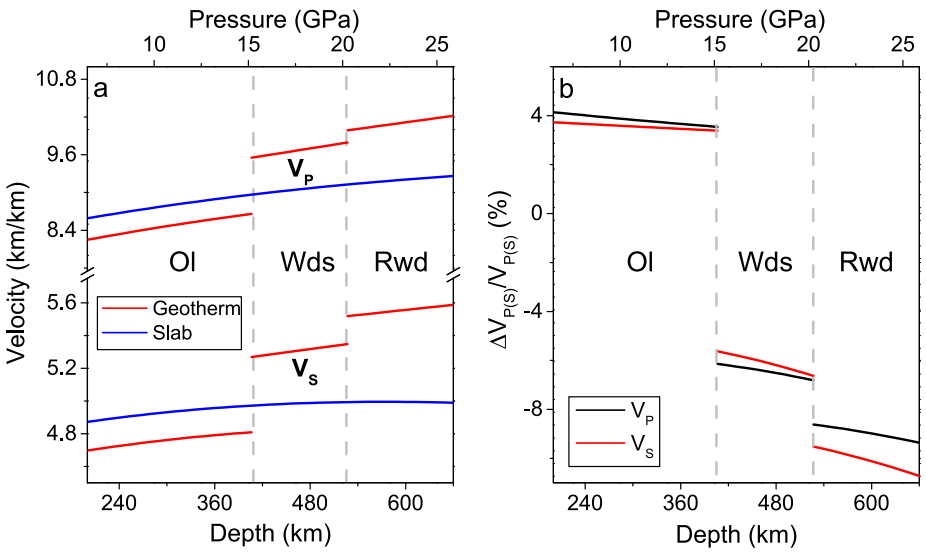

Fig. 7. Compressional (V_P) and shear wave (V_S) velocities of olivine polymorphs in the Earth's mantle. (a) Blue lines: velocities of olivine at 900 K, representing the velocities of olivine in the cold subduction slabs; red lines: velocities of olivine, wadsleyite and ringwoodite along an expected mantle geotherm (Brown and Shankland, 1981). (b) Velocity difference between olivine at 900 K in the slabs and olivine polymorphs along an expected mantle geotherm (Brown and Shankland, 1981). Black line: V_P; red line: V_S. (For interpretation of the references to color in this figure legend, the reader is referred to the web version of this article.)

pleted lherzolite at the bottom (Irifune and Ringwood, 1993; Poli and Schmidt, 2002; Stern, 2002). The volume percentage of olivine is typically greater than 60% in harzburgite and is approximately 40% in lherzolite (Hacker et al., 2003; Poli and Schmidt, 2002; Song et al., 2009; Stern et al., 2012). The relatively low temperatures in the cold slabs will kinetically inhibit the phase transition of olivine to wadsleyite at the depth of 410-km such that olivine in the slabs likely transforms to ringwoodite directly at a greater depth in the transition zone, potentially leading to the occurrence of deep earthquakes at greater than 410-km depth (Chen et al., 2004; Green and Burnley, 1989; Green et al., 1990; Kirby, 1987; Kirby et al., 1996; Mosenfelder et al., 2001; Raterron et al., 2002). If the phase transition of metastable olivine is the major cause for deep earthquakes, the answer to deep earthquakes resides in the seismic signatures and detectability of the metastable olivine wedge. Recently, a number of seismic studies have reported the existence of a low-velocity and anisotropic wedge with 3–5% lower velocities and shear-wave splitting of ~1 s in the slabs below the 410-km depth, which was viewed as evidence for the presence of the metastable olivine in the subducted slabs (e.g. Jiang et al., 2008; Kaneshima et al., 2007; Liu et al., 2008; Pankow et al., 2002; Tono et al., 2009). It is thus of great interest to model the velocity of metastable olivine in the transition zone depth. Comparing the modeled velocity results to seismic observations will provide crucial mineralogical constraints on the seismic signatures of metastable olivine.

Using our new high P–T elasticity results, we have modeled the velocities and anisotropies of the metastable olivine in the cold slabs. Previous studies have shown that the kinetic cut-off temperature for the existence of metastable olivine down to a depth of 600 km is ~873–973 K which is similar to our maximum experimental temperatures (Liu, 1983; Sung and Burns, 1976). Here we assume that the core of the slabs is at 900 K at the transition zone for the computation of the sound velocities of olivine (Fig. 7). Above the 410-km depth, metastable olivine at 900 K has a V_P and V_S ~4% greater than that of an expected normal mantle geotherm. Once the slab crosses the 410-km discontinuity, the V_P and V_S of olivine in the slabs will be ~6% lower than that of wadsleyite in the normal mantle between 410 and 520-km depth and ~8–11% lower than that of ringwoodite between 520 and 660-km depth. Assuming that the olivine content is 60 vol% in the mantle lithosphere as well as in the normal mantle, the velocity in the core of slabs will be ~3.6% lower than that in the normal mantle at 410 to 520-km depth and ~4.8–6.6% lower than that at 520 to 660-km depth. In this case, the presence of metastable olivine in the slabs will produce a seismic signature with lower velocities than the surrounding mantle materials, consistent with a number of seismic observations below the 410-km depth (Iidaka and Suetsugu, 1992; Jiang et al., 2008; Kaneshima et al., 2007).

In addition to the low-velocity wedge in the slabs, seismic anisotropies have also been identified below the 410-km depth (Liu et al., 2008; Sandvol and Ni, 1997; Tono et al., 2009). The observed seismic anisotropy in the slabs in the mantle transition zone could be caused by the preferred alignment of the metastable olivine crystals (Liu et al., 2008; Mainprice, 2007; Sandvol and Ni, 1997; Tono et al., 2009). Using the obtained single-crystal elasticity, we have computed the maximum azimuthal compressional-wave anisotropy, $A_P[(V_{P,\max} - V_{P,\min})/V_{P,\text{ave}}]$, and shear-wave splitting, $A_S^{\text{PO}}[(V_{S2} - V_{S1})/V_{S,\text{ave}}]$, of olivine at various slab temperatures (Fig. 8). In general, olivine has a much greater A_P and A_S^{PO} than that of wadsleyite and ringwoodite along an expected mantle geotherm (Fig. 8). Decreasing temperature only slightly lowers the A_P of olivine. Even if the temperature in the core of slabs is as low as 873 K, the A_P of the metastable olivine in the transition zone is still twice as much as A_P of wadsleyite in the normal mantle and is seven times greater than the A_P of ringwoodite. Meanwhile, we have also noted that A_P calculated using our elasticity of olivine considering the combined P–T effect is greater than those results obtained using literature results (Isaak, 1992; Zha et al., 1998), showing the importance of investigating the elasticity of mantle minerals at simultaneous high P–T conditions relevant to the region.

In contrast to A_P, A_S^{PO} of olivine exhibits a non-linear variation with depth caused by the softening of the shear moduli and the enhanced temperature dependence on the off-diagonal moduli at high pressures (Fig. 8). In particular, A_S^{PO} of olivine along an expected mantle geotherm decreases with depth up to 290-km but starts to increase at greater depths. Such abnormal increase in A_S^{PO} at a greater depth cannot be recognized without the knowledge of the combined P–T effect on the elasticity of single-crystal olivine (Fig. 8). In the cold slabs with a temperature of 873 K where the metastable olivine maybe present, A_S^{PO} will keep de-

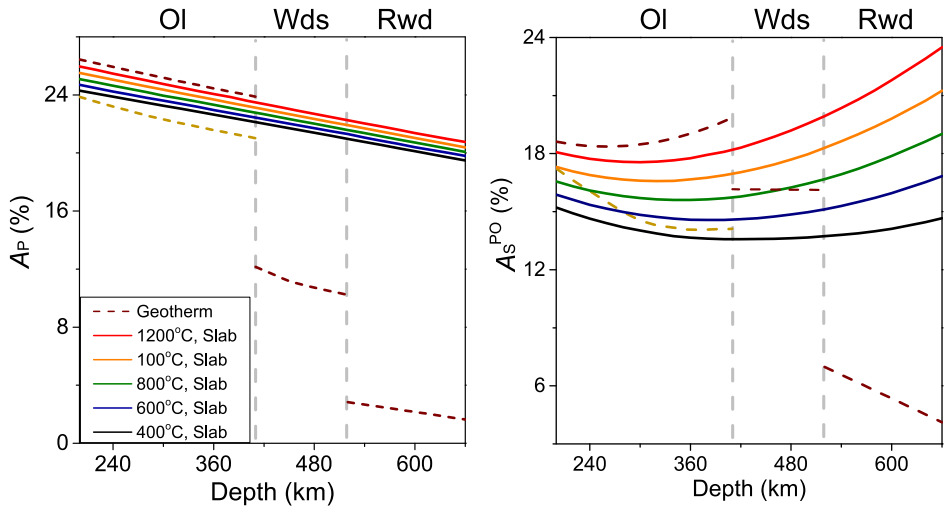

Fig. 8. Velocity anisotropy of olivine at different temperatures in the slab compared with olivine polymorphs along an expected mantle geotherm. (a) Maximum compressional wave anisotropy, A_P. (b) Maximum shear wave splitting, A_S^{PO}. Red, orange, green, blue and black lines: olivine at 1200, 1000, 800, and 600 °C in the slabs, respectively; wine lines: olivine, wadsleyite and ringwoodite along the mantle geotherm (Brown and Shankland, 1981); dark yellow: calculated using the literature high pressure, 300 K and high temperature, 1 bar results of olivine along the mantle geotherm for comparison (Isaak, 1992; Zha et al., 1998). (For interpretation of the references to color in this figure legend, the reader is referred to the web version of this article.)

creasing with increasing depth up to the 410-km discontinuity, but it will become more enhanced in the transition zone region. Along the mantle geotherm, A_S^{PO} of olivine is much greater than that of wadsleyite and ringwoodite. According to our modeled results, the metastable olivine in the cold slabs with a temperature of 873–1273 K has an A_S^{PO} similar to that of wadsleyite in the normal mantle between 410 and 520-km depth. From 520-km depth to the bottom of the transition zone, A_S^{PO} of the metastable olivine is still significantly greater than that of ringwoodite.

Based on the aforementioned discussions, the presence of metastable olivine in the subduction slabs can be used to help explain the observed low-velocity layers and seismic anisotropies in the region. We need to point out that both A_P and A_S^{PO} shown here represent the maximum velocity anisotropies of single-crystal olivine at mantle P–T conditions. Yet modeling the anisotropy of the mantle requires detailed knowledge of the evolution of the lattice preferred orientation (LPO) of polycrystalline olivine with increasing P–T together with our obtained elastic moduli of single-crystal olivine (Mainprice, 2007; Mainprice et al., 2000). However, previous deformation experiments, which provide crucial constraints on the LPO and slip systems of olivine, have been rarely performed at transition zone pressures (e.g. Demouchy et al., 2009; Durham et al., 1977; Faul et al., 2011; Hilairet et al., 2012; Jung and Karato, 2001; Katayama et al., 2004). Even the low pressure and high temperature experiments yield conflicting results (e.g. Demouchy et al., 2009; Durham et al., 2009; Kawazoe et al., 2009; Li et al., 2006). In this case, modeling the anisotropy of subduction slabs using future deformation results for the LPO of olivine at relevant P–T conditions of the transition zone and our elastic moduli of olivine will provide more comprehensive and reliable constraints on the anisotropy of metastable olivine in the slabs.

In summary, the full set of elastic constants of single-crystal olivine has been measured for the first time using combined Brillouin spectroscopy and X-ray diffraction at high P–T conditions. These results provide tight experimental constraints on the combined P–T effects on the sound velocity profiles and seismic anisotropies of olivine in the upper mantle. Although most of the elastic moduli increase with increasing pressure at given high temperatures, three moduli, C_{11}, C_{12} and C_{13} exhibit stronger temperature-induced reduction at greater pressures, showing the importance of the combined effects of high P–T on the elasticity of mantle minerals. The elasticity of single-crystal olivine at high P–T is modeled and applied to decipher the seismic discontinuity at the 410-km depth in a pyrolitic mantle composition as well as the velocity profiles of the metastable olivine wedge in the subduction slabs. Considering the combined high P–T effects on the elasticity of olivine along an expected mantle geotherm, the velocity jumps at the 410-km depth are 6.4% for V_P and 6% for V_S, which are more consistent with seismic observations, although other factors such as the addition of water or compositional effects may still be needed to reconcile the difference between current mineral physics results and seismic observations. We also found that the presence of the metastable olivine in the slabs can exhibit both low velocities and strong seismic anisotropies that are consistent with seismic observations of the region and will help to locate the potential metastable olivine wedge in the slabs. Our in situ high P–T results, together with thermoelastic modeling, provide new insights on the composition and seismic structures of the Earth's mantle.

Acknowledgements

We acknowledge M. Matheney for editing the manuscript. Z. Mao acknowledges support from the National Natural Science Foundation of China (41374092) and the Fundamental Research Funds for the Central Universities in China (WK2080000052). D. Fan acknowledges support from National Natural Science Foundation of China (41374107) and the youth innovative technology talents program of Institute of Geochemistry, Chinese Academy of Sciences. J.F. Lin acknowledges support from the US National Science Foundation (EAR-0838221) and Center for High Pressure Science and Technology Advanced Research. Portions of this work were performed at GeoSoilEnviroCARS, Advanced Photon Source, Argonne National Laboratory, supported by the National Science Foundation (EAR-0622171) and Department of Energy (DE-FG02-94ER14466), under Contract No. DE-AC02-06CH11357.

Appendix A. Supplementary material

Supplementary material related to this article can be found online at http://dx.doi.org/10.1016/j.epsl.2015.06.045.

References

Abramson, E.H., Brown, J.M., Slutsky, L.J., Zaug, J.M., 1997. The elastic constants of San Carlos olivine to 17 GPa. J. Geophys. Res. 102, 12253–12263.

Adams, L.H., 1931. The compressibility of fayalite, and the velocity of elastic waves in peridotite with different iron-magnesium ratio. Beitr. Z. Geophys. 31, 315–321.

Akaogi, M., Ito, E., Navrotsky, A., 1989. Olivine-modified spinel–spinel transitions in the system Mg_2SiO_4–Fe_2SiO_4: calorimetric measurements, thermochemical calculation, and geophysical application. J. Geophys. Res. 94, 15671–15685.

Angel, R.J., Chopelas, A., Ross, N.L., 1992. Stability of high-density clinoenstatite at upper-mantle pressures. Nature 358, 322–324.

Assumpcao, M., Heintz, M., Vauchez, A., Silva, M.E., 2006. Upper mantle anisotropy in SE and Central Brazil from SKS splitting: evidence of asthenospheric flow around a cratonic keel. Earth Planet. Sci. Lett. 250, 224–240.

Bass, J.D., Sinogeikin, S.V., Li, B., 2008. Elastic properties of minerals: a key for understanding the composition and temperature of Earth's interior. Elements 4, 165–170.

Birch, F., 1978. Finite strain isotherm and velocities for single-crystal and polycrystalline NaCl at high-pressures and 300-degree-K. J. Geophys. Res. 83, 1257–1268.

Brown, J.M., Shankland, T.J., 1981. Thermodynamic parameters in the Earth as determined from seismic profiles. Geophys. J. R. Astron. Soc. 66, 579–596.

Cammarano, F., Deuss, A., Goes, S., Giardini, D., 2005a. One-dimensional physical reference models for the upper mantle and transition zone: combining seismic and mineral physics constraints. J. Geophys. Res. 110. http://dx.doi.org/10.1029/2004jb003272.

Cammarano, F., Goes, S., Deuss, A., Giardini, D., 2005b. Is a pyrolitic adiabatic mantle compatible with seismic data? Earth Planet. Sci. Lett. 232, 227–243.

Cammarano, F., Goes, S., Vacher, P., Giardini, D., 2003. Inferring upper-mantle temperatures from seismic velocities. Phys. Earth Planet. Inter. 138, 197–222.

Chai, M., Brown, J.M., Slutsky, L.J., 1997. The elastic constants of an aluminous orthopyroxene to 12.5 GPa. J. Geophys. Res. 102, 14779–14785.

Chen, M., El Goresy, A., Gillet, P., 2004. Ringwoodite lamellae in olivine: clues to olivine–ringwoodite phase transition mechanisms in shocked meteorites and subducting slabs. Proc. Natl. Acad. Sci. USA 101, 15033–15037.

Chen, W.P., Brudzinski, M.R., 2003. Seismic anisotropy in the mantle transition zone beneath Fiji–Tonga. Geophys. Res. Lett. 30. http://dx.doi.org/10.1029/2002gl016330.

Collins, M.D., Brown, J.M., 1998. Elasticity of an upper mantle clinopyroxene. Phys. Chem. Miner. 26, 7–13.

Demouchy, S., Schneider, S.E., Mackwell, S.J., Zimmerman, M.E., Kohlstedt, D.L., 2009. Experimental deformation of olivine single crystals at lithospheric temperatures. Geophys. Res. Lett. 36. http://dx.doi.org/10.1029/2008gl036611.

Duffy, T.S., Anderson, D.L., 1989. Seismic velocities in mantle minerals and the mineralogy of the upper mantle. J. Geophys. Res. 94, 1895–1912.

Duffy, T.S., Zha, C.S., Downs, R.T., Mao, H.K., Hemley, R.J., 1995. Elasticity of forsterite to 16 GPa and the composition of the upper-mantle. Nature 378, 170–173.

Durham, W.B., Goetze, C., Blake, B., 1977. Plastic-flow of oriented single-crystals of olivine. 2. Observations and interpretations of dislocation-structures. J. Geophys. Res. 82, 5755–5770.

Durham, W.B., Mei, S., Kohlstedt, D.L., Wang, L., Dixon, N.A., 2009. New measurements of activation volume in olivine under anhydrous conditions. Phys. Earth Planet. Inter. 172, 67–73.

Dziewonski, A.M., Anderson, D.L., 1981. Preliminary reference Earth model. Phys. Earth Planet. Inter. 25, 297–356.

Ekstrom, G., Dziewonski, A.M., 1998. The unique anisotropy of the Pacific upper mantle. Nature 394, 168–172.

Every, A.G., 1980. General closed-form expressions for acoustic-waves in elastically anisotropic solids. Phys. Rev. B 22, 1746–1760.

Fan, D., Mao, Z., Yang, J., Lin, J.-F., accepted. Determination of the full elastic tensor of single crystals using shear wave velocities by Brillouin spectroscopy. Am. Mineral.

Faul, U.H., Gerald, J.D.F., Farla, R.J.M., Ahlefeldt, R., Jackson, I., 2011. Dislocation creep of fine-grained olivine. J. Geophys. Res. 116. http://dx.doi.org/10.1029/2009jb007174.

Fei, Y., Bertka, C.M., 1999. Phase transitions in the Earth's mantle and mantle mineralogy. In: Fei, Y., Bertka, C.M., Mysen, B.O. (Eds.), Mantle Petrology: Field Observations and High Pressure Experimentation. A Tribute to Francis R. (Joe) Boyd. The Geochemical Society Special Publications, Houston, TX, pp. 189–207.

Fei, Y.W., Ricolleau, A., Frank, M., Mibe, K., Shen, G.Y., Prakapenka, V., 2007. Toward an internally consistent pressure scale. Proc. Natl. Acad. Sci. USA 104, 9182–9186.

Finger, L.W., Ohashi, Y., 1976. Thermal-expansion of diopside to 800 °C and a refinement of crystal-structure at 700 °C. Am. Mineral. 61, 303–310.

Frost, D.J., 2003. The structure and sharpness of $(Mg,Fe)_2SiO_4$ phase transformations in the transition zone. Earth Planet. Sci. Lett. 216, 313–328.

Grand, S.P., Helmberger, D.V., 1984. Upper mantle shear structure of North-America. Geophys. J. R. Astron. Soc. 76, 399–438.

Green, H.W., Burnley, P.C., 1989. A new self-organizing mechanism for deep-focus earthquakes. Nature 341, 733–737.

Green, H.W., Chen, W.P., Brudzinski, M.R., 2010. Seismic evidence of negligible water carried below 400-km depth in subducting lithosphere. Nature 467, 828–831.

Green, H.W., Houston, H., 1995. The mechanics of deep earthquakes. Annu. Rev. Earth Planet. Sci. 23, 169–213.

Green, H.W., Young, T.E., Walker, D., Scholz, C.H., 1990. Anticrack-associated faulting at very high-pressure in natural olivine. Nature 348, 720–722.

Hacker, B.R., Abers, G.A., Peacock, S.M., 2003. Subduction factory – 1. Theoretical mineralogy, densities, seismic wave speeds, and H_2O contents. J. Geophys. Res. 108. http://dx.doi.org/10.1029/2001jb001127.

Hilairet, N., Wang, Y.B., Sanehira, T., Merkel, S., Mei, S.M., 2012. Deformation of olivine under mantle conditions: an in situ high-pressure, high-temperature study using monochromatic synchrotron radiation. J. Geophys. Res. 117. http://dx.doi.org/10.1029/2011jb008498.

Iidaka, T., Suetsugu, D., 1992. Seismological evidence for metastable olivine inside a subducting slab. Nature 356, 593–595.

Irifune, T., 1987. An experimental investigation of the pyroxene garnet transformation in a pyrolite composition and its bearing on the constitution of the mantle. Phys. Earth Planet. Inter. 45, 324–336.

Irifune, T., Higo, Y., Inoue, T., Kono, Y., Ohfuji, H., Funakoshi, K., 2008. Sound velocities of majorite garnet and the composition of the mantle transition region. Nature 451, 814–817.

Irifune, T., Isshiki, M., 1998. Iron partitioning in a pyrolite mantle and the nature of the 410-km seismic discontinuity. Nature 392, 702–705.

Irifune, T., Ringwood, A.E., 1987. Phase transformations in primitive MORB and pyrolite compositions to 25 GPa and some geophysical implications. In: Syono, Y., Manghnani, M.H. (Eds.), High-Pressure Research in Mineral Physics. American Geophysical Union, Washington D.C., pp. 231–242.

Irifune, T., Ringwood, A.E., 1993. Phase transformations in subducted oceanic crust and buoyancy relationships at depths of 600–800 km in the mantle. Earth Planet. Sci. Lett. 117, 101–110.

Isaak, D.G., 1992. High-temperature elasticity of iron-bearing olivines. J. Geophys. Res. 97, 1871–1885. http://dx.doi.org/10.1029/91jb02675.

Isaak, D.G., Gwanmesia, G.D., Davis, M.G., Stafford, S.C., Stafford, A.M., Triplett, R.S., 2010. The temperature dependence of the elasticity of Fe-bearing wadsleyite. Phys. Earth Planet. Inter. 182, 107–112. http://dx.doi.org/10.1016/j.pepi.2010.06.014.

Isaak, D.G., Gwanmesia, G.D., Falde, D., Davis, M.G., Triplett, R.S., Wang, L.P., 2007. The elastic properties of beta-Mg_2SiO_4 from 295 to 660 K and implications on the composition of Earth's upper mantle. Phys. Earth Planet. Inter. 162, 22–31.

Ita, J., Stixrude, L., 1992. Petrology, elasticity, and composition of the mantle transition zone. J. Geophys. Res. 97, 6849–6866.

Jackson, J.M., Palko, J.W., Andrault, D., Sinogeikin, S.V., Lakshtanov, D.L., Wang, J.Y., Bass, J.D., Zha, C.S., 2003. Thermal expansion of natural orthoenstatite to 1473 K. Eur. J. Mineral. 15, 469–473.

Jackson, J.M., Sinogeikin, S.V., Bass, J.D., 2007. Sound velocities and single-crystal elasticity of orthoenstatite to 1073 K at ambient pressure. Phys. Earth Planet. Inter. 161, 1–12.

Jacobsen, S.D., Jiang, F.M., Mao, Z., Duffy, T.S., Smyth, J.R., Holl, C.M., Frost, D.J., 2008. Effects of hydration on the elastic properties of olivine. Geophys. Res. Lett. 35. http://dx.doi.org/10.1029/2008gl034398.

Jeanloz, R., Thompson, A.B., 1983. Phase transitions and mantle discontinuities. Rev. Geophys. 21, 51–74.

Jiang, F., Speziale, S., Duffy, T.S., 2006. Single-crystal elasticity of brucite, $Mg(OH)_2$, to 15 GPa by Brillouin scattering. Am. Mineral. 91, 1893–1900.

Jiang, F.M., Speziale, S., Duffy, T.S., 2004a. Single-crystal elasticity of grossular- and almandine-rich garnets to 11 GPa by Brillouin scattering. J. Geophys. Res. 109. http://dx.doi.org/10.1029/2004jb003081.

Jiang, F.M., Speziale, S., Shieh, S.R., Duffy, T.S., 2004b. Single-crystal elasticity of andradite garnet to 11 GPa. J. Phys. Condens. Matter 16, S1041–S1052. http://dx.doi.org/10.1088/0953-8984/16/14/014.

Jiang, G.M., Zhao, D.P., Zhang, G.B., 2008. Seismic evidence for a metastable olivine wedge in the subducting Pacific slab under Japan Sea. Earth Planet. Sci. Lett. 270, 300–307.

Jung, H., Karato, S., 2001. Water-induced fabric transitions in olivine. Science 293, 1460–1463.

Jung, H., Mo, W., Green, H.W., 2009. Upper mantle seismic anisotropy resulting from pressure-induced slip transition in olivine. Nat. Geosci. 2, 73–77.

Kaneshima, S., Okamoto, T., Takenaka, H., 2007. Evidence for a metastable olivine wedge inside the subducted Mariana slab. Earth Planet. Sci. Lett. 258, 219–227.

Kantor, I., Prakapenka, V., Kantor, A., Dera, P., Kurnosov, A., Sinogeikin, S., Dubrovinskaia, N., Dubrovinsky, L., 2012. BX90: a new diamond anvil cell design for X-ray diffraction and optical measurements. Rev. Sci. Instrum. 83. http://dx.doi.org/10.1063/1.4768541.

Karato, S., 1993. Importance of anelasticity in the interpretation of seismic tomography. Geophys. Res. Lett. 20, 1623–1626.

Karato, S., Jung, H., Katayama, I., Skemer, P., 2008. Geodynamic significance of seismic anisotropy of the upper mantle: new insights from laboratory studies. Annu. Rev. Earth Planet. Sci. 36, 59–95.

Katayama, I., Jung, H., Karato, S.I., 2004. New type of olivine fabric from deformation experiments at modest water content and low stress. Geology 32, 1045–1048.

Katsura, T., Ito, E., 1989. The system Mg_2SiO_4–Fe_2SiO_4 at high-pressures and temperatures: precise determination of stabilities of olivine, modified spinel, and spinel. J. Geophys. Res. 94, 15663–15670.
Kawazoe, T., Karato, S., Otsuka, K., Jing, Z.C., Mookherjee, M., 2009. Shear deformation of dry polycrystalline olivine under deep upper mantle conditions using a rotational Drickamer apparatus (RDA). Phys. Earth Planet. Inter. 174, 128–137.
Kennett, B.L.N., Engdahl, E.R., Buland, R., 1995. Constraints on seismic velocities in the Earth from travel-times. Geophys. J. Int. 122, 108–124.
Kirby, S., 1995. Interslab earthquakes and phase-changes in subducting lithosphere. Rev. Geophys. 33, 287–297.
Kirby, S.H., 1987. Localized polymorphic phase-transformations in high-pressure faults and applications to the physical-mechanism of deep earthquakes. J. Geophys. Res. 92, 13789–13800.
Kirby, S.H., Stein, S., Okal, E.A., Rubie, D.C., 1996. Metastable mantle phase transformations and deep earthquakes in subducting oceanic lithosphere. Rev. Geophys. 34, 261–306.
Kung, J., Li, B.S., 2014. Lattice dynamic behavior of orthoferrosilite ($FeSiO_3$) toward phase transition under compression. J. Phys. Chem. C 118, 12410–12419.
Kung, J., Li, B.S., Uchida, T., Wang, Y.B., 2005. In-situ elasticity measurement for the unquenchable high-pressure clinopyroxene phase: implication for the upper mantle. Geophys. Res. Lett. 32. http://dx.doi.org/10.1029/2004gl021661.
Lefevre, L.V., 1989. Upper mantle P velocity structure of the Canadian shield. J. Geophys. Res. 94, 17749–17765.
Li, B., Liebermann, R.C., 2007. Indoor seismology by probing the Earth's interior by using sound velocity measurements at high pressures and temperatures. Proc. Natl. Acad. Sci. USA 104, 9145–9150.
Li, B., Liebermann, R.C., Weidner, D.J., 2001. P–V–V_P–V_S–T measurements on wadsleyite to 7 GPa and 873 K: implications for the 410-km seismic discontinuity. J. Geophys. Res. 106, 30579–30591.
Li, B.S., Kung, J., Liu, W., Liebermann, R.C., 2014. Phase transition and elasticity of enstatite under pressure from experiments and first-principles studies. Phys. Earth Planet. Inter. 228, 63–74.
Li, L.L., Weidner, D., Raterron, P., Chen, J.H., Vaughan, M., Me, S.H., Durham, B., 2006. Deformation of olivine at mantle pressure using the D-DIA. Eur. J. Mineral. 18, 7–19.
Liu, K.H., Gao, S.S., Gao, Y., Wu, J., 2008. Shear wave splitting and mantle flow associated with the deflected Pacific slab beneath northeast Asia. J. Geophys. Res. 113. http://dx.doi.org/10.1029/2007jb005178.
Liu, L.G., 1983. Phase transformations, earthquakes and the descending lithosphere. Phys. Earth Planet. Inter. 32, 226–240.
Liu, W., Kung, J., Li, B.S., 2005. Elasticity of San Carlos olivine to 8 GPa and 1073 K. Geophys. Res. Lett. 32. http://dx.doi.org/10.1029/2005gl023453.
Liu, W., Li, B.S., 2006. Thermal equation of state of $(Mg_{0.9}Fe_{0.1})_2SiO_4$ olivine. Phys. Earth Planet. Inter. 157, 188–195.
Long, M.D., Becker, T.W., 2010. Mantle dynamics and seismic anisotropy. Earth Planet. Sci. Lett. 297, 341–354.
Long, M.D., van der Hilst, R.D., 2005. Upper mantle anisotropy beneath Japan from shear wave splitting. Phys. Earth Planet. Inter. 151, 206–222.
Lu, C., Mao, Z., Lin, J.F., Zhuravlev, K.K., Tkachev, S.N., Prakapenka, V.B., 2013. Elasticity of single-crystal iron-bearing pyrope up to 20 GPa and 750 K. Earth Planet. Sci. Lett. 361, 134–142.
Mainprice, D., 2007. Seismic anisotropy of the deep Earth from a mineral and rock physics properties. In: Schubert, G. (Ed.), Treatise on Geophysics. Elsevier Ltd., Oxford, pp. 437–491.
Mainprice, D., Barruol, G., Ismail, W.B., 2000. The seismic anisotropy of the Earth's mantle: from single-crystal to polycrystal. In: Karato, S., Forte, A., Lieberma, R., Masters, G., Stixrude, L. (Eds.), Earth's Deep Interior: Mineral Physics and Tomography from the Atomic to the Global Scale. American Geophysical Union, pp. 237–264.
Mainprice, D., Tommasi, A., Couvy, H., Cordier, P., Frost, D.J., 2005. Pressure sensitivity of olivine slip systems and seismic anisotropy of Earth's upper mantle. Nature 433, 731–733.
Mao, H.K., Xu, J., Bell, P.M., 1986. Calibration of the ruby pressure gauge to 800-kbar under quasi-hydrostatic conditions. J. Geophys. Res. 91, 4673–4676.
Mao, Z., Jacobsen, S.D., Frost, D.J., McCammon, C.A., Hauri, E.H., Duffy, T.S., 2011. Effect of hydration on the single-crystal elasticity of Fe-bearing wadsleyite to 12 GPa. Am. Mineral. 96, 1606–1612.
Mao, Z., Jacobsen, S.D., Jiang, F., Smyth, J.R., Holl, C.M., Duffy, T.S., 2008a. Elasticity of hydrous wadsleyite to 12 GPa: implications for Earth's transition zone. Geophys. Res. Lett. 35. http://dx.doi.org/10.1029/2008gl035618.
Mao, Z., Jacobsen, S.D., Jiang, F.M., Smyth, J.R., Holl, C.M., Frost, D.J., Duffy, T.S., 2008b. Single-crystal elasticity of wadsleyites, beta-Mg_2SiO_4, containing 0.37–1.66 wt.% H_2O. Earth Planet. Sci. Lett. 268, 540–549.
Mao, Z., Jacobsen, S.D., Jiang, F., Smyth, J.R., Holl, C.M., Frost, D.J., Duffy, T.S., 2010. Velocity crossover between hydrous and anhydrous forsterite at high pressures. Earth Planet. Sci. Lett. 293, 250–258. http://dx.doi.org/10.1016/j.epsl.2010.02.025.
Mao, Z., Jiang, F.M., Duffy, T.S., 2007. Single-crystal elasticity of zoisite $Ca_2Al_3Si_3O_{12}(OH)$ by Brillouin scattering. Am. Mineral. 92, 570–576.
Marone, F., Romanowicz, B., 2007. The depth distribution of azimuthal anisotropy in the continental upper mantle. Nature 447, 198–201.
Marquardt, H., Speziale, S., Reichmann, H.J., Frost, D.J., Schilling, F.R., Garnero, E.J., 2009. Elastic shear anisotropy of ferropericlase in Earth's lower mantle. Science 324, 224–226.
Mosenfelder, J.L., Marton, F.C., Ross, C.R., Kerschhofer, L., Rubie, D.C., 2001. Experimental constraints on the depth of olivine metastability in subducting lithosphere. Phys. Earth Planet. Inter. 127, 165–180.
Murakami, M., Ohishi, Y., Hirao, N., Hirose, K., 2012. A perovskitic lower mantle inferred from high-pressure, high-temperature sound velocity data. Nature 485, 90-U118. http://dx.doi.org/10.1038/Nature11004.
Nettles, M., Dziewonski, A.M., 2008. Radially anisotropic shear velocity structure of the upper mantle globally and beneath North America. J. Geophys. Res. 113. http://dx.doi.org/10.1029/2006jb004819.
Nunez-Valdez, M., Umemoto, K., Wentzcovitch, R.M., 2010. Fundamentals of elasticity of $(Mg_{1-x},Fe_x)_2SiO_4$ olivine. Geophys. Res. Lett. 37. http://dx.doi.org/10.1029/2010gl044205.
Pacalo, R.E.G., Gasparik, T., 1990. Reversals of the orthoenstatite–clinoenstatite transition at high-pressures and high-temperatures. J. Geophys. Res. 95, 15853–15858.
Pankow, K.L., Williams, Q., Lay, T., 2002. Using shear wave amplitude patterns to detect metastable olivine in subducted slabs. J. Geophys. Res. 107. http://dx.doi.org/10.1029/2001jb000608.
Pearson, D.G., Brenker, F.E., Nestola, F., McNeill, J., Nasdala, L., Hutchison, M.T., Matveev, S., Mather, K., Silversmit, G., Schmitz, S., Vekemans, B., Vincze, L., 2014. Hydrous mantle transition zone indicated by ringwoodite included within diamond. Nature 507, 221–224.
Poli, S., Schmidt, M.W., 2002. Petrology of subducted slabs. Annu. Rev. Earth Planet. Sci. 30, 207–235.
Raterron, P., Chen, J.H., Weidner, D.J., 2002. A process for low-temperature olivine-spinel transition under quasi-hydrostatic stress. Geophys. Res. Lett. 29. http://dx.doi.org/10.1029/2002gl015003.
Ringwood, A.E., 1975. Composition and Petrology of the Earth's Mantle. McGraw-Hill, New York.
Romanowicz, B., 1991. Seismic tomography of the Earth's mantle. Annu. Rev. Earth Planet. Sci. 19, 77–99.
Romanowicz, B., Durek, J.J., 2000. Seismological constraints on attenuation in the Earth: a review. In: Karato, S., Forte, A., Liebermann, R.C. (Eds.), Earth's Deep Interior: Mineral Physics and Tomography from the Atomic to the Global Scale. American Geophysical Union, Washington D.C., pp. 161–179.
Sandvol, E., Ni, J., 1997. Deep azimuthal seismic anisotropy in the southern Kurile and Japan subduction zones. J. Geophys. Res. 102, 9911–9922.
Sang, L.Q., Bass, J.D., 2014. Single-crystal elasticity of diopside to 14 GPa by Brillouin scattering. Phys. Earth Planet. Inter. 228, 75–79.
Schmandt, B., Jacobsen, S.D., Becker, T.W., Liu, Z., Dueker, K.G., 2014. Dehydration melting at the top of the lower mantle. Science 344, 1265–1268.
Sinogeikin, S.V., Bass, J.D., 2000. Single-crystal elasticity of pyrope and MgO to 20 GPa by Brillouin scattering in the diamond cell. Phys. Earth Planet. Inter. 120, 43–62.
Sinogeikin, S.V., Bass, J.D., 2002. Elasticity of pyrope and majorite–pyrope solid solutions to high temperatures. Earth Planet. Sci. Lett. 203, 549–555.
Sinogeikin, S.V., Bass, J.D., Katsura, T., 2001. Single-crystal elasticity of gamma-$(Mg_{0.91}Fe_{0.09})_2SiO_4$ to high pressures and to high temperatures. Geophys. Res. Lett. 28, 4335–4338.
Sinogeikin, S.V., Bass, J.D., Katsura, T., 2003. Single-crystal elasticity of ringwoodite to high pressures and high temperatures: implications for 520 km seismic discontinuity. Phys. Earth Planet. Inter. 136, 41–66.
Sinogeikin, S.V., Katsura, T., Bass, J.D., 1998. Sound velocities and elastic properties of Fe-bearing wadsleyite and ringwoodite. J. Geophys. Res. 103, 20819–20825.
Song, S.G., Su, L., Niu, Y.L., Zhang, G.B., Zhang, L.F., 2009. Two types of peridotite in North Qaidam UHPM belt and their tectonic implications for oceanic and continental subduction: a review. J. Asian Earth Sci. 35, 285–297.
Song, T.R.A., Helmberger, D.V., Grand, S.P., 2004. Low-velocity zone atop the 410-km seismic discontinuity in the northwestern United States. Nature 427, 530–533.
Speziale, S., Duffy, T.S., 2002. Single-crystal elastic constants of fluorite (CaF_2) to 9.3 GPa. Phys. Chem. Miner. 29, 465–472.
Speziale, S., Duffy, T.S., Angel, R.J., 2004. Single-crystal elasticity of fayalite to 12 GPa. J. Geophys. Res. 109. http://dx.doi.org/10.1029/2004jb003162.
Stern, R.J., 2002. Subduction zones. Rev. Geophys. 40. http://dx.doi.org/10.1029/2001rg000108.
Stern, R.J., Reagan, M., Ishizuka, O., Ohara, Y., Whattam, S., 2012. To understand subduction initiation, study forearc crust: to understand forearc crust, study ophiolites. Lithosphere 4, 469–483.
Stixrude, L., Lithgow-Bertelloni, C., 2005. Mineralogy and elasticity of the oceanic upper mantle: origin of the low-velocity zone. J. Geophys. Res. 110. http://dx.doi.org/10.1029/2004jb002965.
Sung, C.M., Burns, R.G., 1976. Kinetics of high-pressure phase transformations: implications to evolution of olivine-spinel transition in downgoing lithosphere and its consequences on dynamics of mantle. Tectonophysics 31, 1–32.
Tono, Y., Fukao, Y., Kunugi, T., Tsuboi, S., 2009. Seismic anisotropy of the Pacific slab and mantle wedge beneath the Japanese islands. J. Geophys. Res. 114. http://dx.doi.org/10.1029/2009jb006290.

van der Hilst, R.D., de Hoop, M.V., Wang, P., Shim, S.H., Ma, P., Tenorio, L., 2007. Seismostratigraphy and thermal structure of Earth's core–mantle boundary region. Science 315, 1813–1817.

van der Meijde, M., Marone, F., Giardini, D., van der Lee, S., 2003. Seismic evidence for water deep in earth's upper mantle. Science 300, 1556–1558.

Walck, M.C., 1985. The upper mantle beneath the northeast Pacific rim: a comparison with the Gulf of California. Geophys. J. R. Astron. Soc. 81, 243–276.

Wang, J.Y., Bass, J.D., Kastura, T., 2014. Elastic properties of iron-bearing wadsleyite to 17.7 GPa: implications for mantle mineral models. Phys. Earth Planet. Inter. 228, 92–96.

Webb, S.L., 1989. The elasticity of the upper mantle orthosilicates olivine and garnet to 3 GPa. Phys. Chem. Miner. 16, 684–692.

Xu, W.B., Lithgow-Bertelloni, C., Stixrude, L., Ritsema, J., 2008. The effect of bulk composition and temperature on mantle seismic structure. Earth Planet. Sci. Lett. 275, 70–79.

Yang, R., Wu, Z., 2014. Elastic properties of stishovite and the $CaCl_2$-type silica at the mantle temperature and pressure: an ab initio investigation. Earth Planet. Sci. Lett. 404, 14–21.

Zha, C.S., Duffy, T.S., Downs, R.T., Mao, H.K., Hemley, R.J., 1996. Sound velocity and elasticity of single-crystal forsterite to 16 GPa. J. Geophys. Res. 101, 17535–17545.

Zha, C.S., Duffy, T.S., Downs, R.T., Mao, H.K., Hemley, R.J., 1998. Brillouin scattering and X-ray diffraction of San Carlos olivine: direct pressure determination to 32 GPa. Earth Planet. Sci. Lett. 159, 25–33.

Zha, C.S., Duffy, T.S., Mao, H.K., Downs, R.T., Hemley, R.J., Weidner, D.J., 1997. Single-crystal elasticity of beta-Mg_2SiO_4 to the pressure of the 410 km seismic discontinuity in the Earth's mantle. Earth Planet. Sci. Lett. 147 (E9–E15). http://dx.doi.org/10.1016/S0012-821x(97)00010-1.

Zhao, Y.S., VonDreele, R.B., Shankland, T.J., Weidner, D.J., Zhang, J.Z., Wang, Y.B., Gasparik, T., 1997. Thermoelastic equation of state of jadeite $NaAlSi_2O_6$: an energy-dispersive Reitveld refinement study of low symmetry and multiple phases diffraction. Geophys. Res. Lett. 24, 5–8.

Zou, Y.T., Greaux, S., Irifune, T., Whitaker, M.L., Shinmei, T., Higo, Y., 2012. Thermal equation of state of $Mg_3Al_2Si_3O_{12}$ pyrope garnet up to 19 GPa and 1700 K. Phys. Chem. Miner. 39, 589–598.